J Indian Inst. Sci., Nov.–Dec. 1989, **69**, 457–484

IISc THESES ABSTRACTS

Thesis Abstract (Ph.D.)

The Wiener-Hopf technique and allied methods in a class of scattering problems by S. Dowerah.
Research supervisor: A. Chakrabarti.
Department: Applied Mathematics.

1. Introduction

The Wiener-Hopf technique in its standard form and the approximate methods based on it serve as extremely powerful tools for attacking a wide class of boundary-value problems associated with certain elliptic and parabolic-type partial differential equations. Such boundary-value problems arise in scattering of electromagnetic and acoustic waves and in various other branches of mathematical physics such as surface water-wave theory, electrodynamics, radiative energy transfer, diffusion phenomena, etc. Recently, various modifications of this technique have been proposed to handle 2×2 coupled Wiener-Hopf systems arising in diffraction theory. This thesis presents a detailed investigation of radiation and scattering of electromagnetic and acoustic waves by various geometrical structures with the help of the Wiener-Hopf technique, its various generalizations and modifications, and related methods.

2. The class of scattering problems

As applications of the Wiener-Hopf theory, various authors have considered diffraction problems associated with a single half-plane, a pair or series of parallel half-planes, a strip and with other geometrical configurations under different boundary conditions. But all these problems are basically problems of plane boundaries and no satisfactory attempt seems to exist to tackle diffraction problems associated with uneven boundaries by the Wiener-Hopf technique or its modifications. Accordingly, a class of scattering problems associated with obstacles involving small amplitude sinusoidally perturbed boundaries is investigated in the present work. The problem of diffraction of a plane wave by two unstaggered parallel corrugated half-planes involves the use of the Wiener-Hopf technique and a suitably designed perturbation scheme (for details see our paper[1]). The solution to the corresponding problem associated with a single half-plane is obtained as a limiting case by allowing the spacing between the perturbed half-planes to tend to zero. The problem of diffraction by a single corrugated strip is formulated in terms of a three-part Wiener-Hopf equation which is next reduced to integral equations of special type. These integral equations are approximately solved under the assumption that the ratio of the width of the strip to the wavelength is a large quantity (for details we refer to our paper[2]). The scattered field produced by a single periodically perturbed half-plane under plane wave excitation is utilized to investigate, in the high-frequency limit, the diffraction problem for a plane electromagnetic wave falling on two staggered parallel half-planes with periodic wall perturbations (for a detailed analysis see our paper[3]). Known results are obtained as particular cases

of the general situations considered. Analytical expressions are presented for various physical quantities. A considerable body of knowledge about the effect of wall perturbations on the scattered field can be built up from these expressions.

The field produced by the diffraction of two knife edges of a plane acoustic wave of short wavelength is also determined by the Wiener-Hopf technique and the results are compared with the predictions of the uniform asymptotic theory of diffraction as demonstrated by Ahluwaliah *et al*[4] and clarified by Boersma[5] in the circumstances when mixed boundary conditions are prescribed on one of the scatterers (see our paper[6]). The case when the incident ray is not parallel to the line joining the two edges and the case when the incident ray grazes over the two edges are considered separately. In both the cases the rigorous asymptotic expansion of the solution obtained by the Wiener-Hopf technique is found to be in agreement with the formal asymptotic solution provided by the uniform asymptotic theory of diffraction. The analysis is extended to the case when mixed boundary conditions (a Neumann condition on the bottom surface and a Dirichlet condition on the top surface *i.e.* soft/hard) are prescribed on both the half-planes.

The problem of diffraction of a plane acoustic wave by two unstaggered mixed-type parallel half-planes is next considered for its solution. This problem leads to a system of 4×4 Wiener-Hopf equations which is separated into two independent 2×2 Wiener-Hopf systems. It does not seem possible to solve these two Wiener-Hopf systems by direct matrix factorization techniques. An approach aiming to bypass the construction of appropriate matrix Wiener-Hopf factors is therefore adopted and the problem of solving these two Wiener-Hopf systems is next reduced to that of solving two independent standard Wiener-Hopf equations involving unknown constants. The solutions of these two Wiener-Hopf equations ultimately determine the solutions of the original Wiener-Hopf systems explicitly in terms of constants satisfying two independent linear algebraic systems of equations. An analytical expression for the total field inside the duct formed by the half-planes satisfying the desired boundary condition on the inner surfaces is derived. Uniformly valid asymptotic form of the total acoustic field outside the half-planes is also presented.

An explicit solution to the diffraction problem by three equidistant half-planes is obtained by avoiding complicated analysis encountered in approaching this particular problem for its solution through the matrix factorization technique. If the spacing between the half-planes is less than one fourth of the wavelength all other waveguide modes are found to be cut-off and the field in each waveguide is ultimately determined by the travelling wave terms.

A special class of 2×2 matrix Wiener-Hopf problems is considered for solution through a singular integral equation of a particular type[7,8]. The present analysis uses the factorization of the elements of the matrix in question instead of the matrix itself. Two important and known particular cases of this class of 2×2 matrix Wiener-Hopf problems are considered at the end to substantiate the validity of this approach.

The last problem in the thesis is that of scattering of a transverse electric wave by a dielectric strip of electrically small thickness[9]. The problem is formulated in terms of an uncoupled system of three-part Wiener-Hopf equations by using a set of approximate boundary conditions derived and utilized recently[10,11]. The resulting perturbed Wiener-Hopf equations are solved approximately for electrically large width of the strip by using Jones' method[1]. An analytical formula is derived for the extinction cross-section of the strip. The radar cross-section is also computed and variations of both the important physical quantities with respect to the angle of incidence are studied in special situations. Whilst all the analytical results have been finally expressed in neat computable forms in most of the problems studied in the thesis, numerical results have also been determined for certain practical quantities, *e.g.* the scattering cross-section and the radar cross-section of the dielectric strip.

References

1. CHAKRABARTI, A. AND DOWERAH, S. *Can. J. Phys.*, 1984, **62**, 271–284.
2. CHAKRABARTI, A. AND DOWERAH, S. *J. Tech. Phys.*, 1984, **25**, 113–126
3. DOWERAH, S. AND CHAKRABARTI, A. *Indian J. Pure Appl. Math.*, 1985, **16**, 411–447.
4. AHLUWALIA, D. S., LEWIS, P. M. AND BOERSMA, J. *SIAM J. Appl. Math*, 1968, **16**, 783–807.
5. BOERSMA, J. *Q. J. Mech. Appl. Math.*, 1975, **28**, 405–425.
6. DOWERAH, S. AND CHAKRABARTI, A. *J. Sound Vibr.*, 1987, **116**, 49–70.
7. PETERS, A. S *Commun. Pure Appl. Math.*, 1972, **25**, 369–402.
8. CHAKRABARTI, A. *J. Indian Inst. Sci. (B)*, 1984, **65**, 179–183.
9. DOWERAH, S. AND CHAKRABARTI, A. *IEEE Trans.*, 1988, **AP-36**, 696–706.
10. LEPPINGTON, F. G. *Proc. R. Soc. Lond. A*, 1983, **386**, 443–460.
11. CHAKRABARTI, A *IEEE Trans*, 1986, **AP-34**, 830–833.

Thesis Abstract (Ph.D.)

Computations in linear algebra: A new look at residue arithmetic by V. Ch. Venkaiah.
Research supervisors: A. Ramachandra Rao, P. S. Naidu and S. K. Sen.
Department: Applied Mathematics.

1. Introduction

The exact and approximate computations of some linear algebraic problems with an emphasis on a modified residue arithmetic developed here are dealt with in this thesis.

The conventional multiple modulus residue arithmetic[1] fails in case a denominator of a rational operand or a divisor in a division operation happens to be an integral multiple of one or more moduli. In this case the computation needs to be started afresh with respect to a modulus. A similar problem exists when the residue arithmetic is used for computation with operands which are rational functions. This problem is overcome in this thesis by modifying the existing residue arithmetic. Also, considered here are applications of these arithmetic to two types of linear algebraic problems. Further, it is shown that the residue arithmetic cannot be superimposed on all the algorithms of a linear algebraic problems by considering a polynomial time algorithm due to Barnes[2] which is a variation on Karmarkar's algorithm.

2. Main results

A modified residue number system in which each residue number is represented as an ordered pair (mantissa, exponent) and the concerned arithmetic, named here as floating-point modular arithmetic

for numbers (FLMAN), are described for error-free computation with rational operands. The division operation in this number system, unlike that in the existing number systems, can be carried out even when the denominator of a rational operand or the divisor in a division operation happens to be an integral multiple of one or more moduli. In addition, an algorithm, alternative to Gregory's algorithm[3], that defines an extended set of Farey fractions, called here as generalized Farey traditions, is proposed to convert residue numbers to rational numbers. The foregoing FLMAN has been extended to rational functions in which the elements of the base vector are irreducible polynomials. The Lagrange interpolation formula is used in place of the Chinese remainder theorem for polynomials. An algorithm for arithmetic on rational functions including a forward mapping, the floating-point modular arithmetic, the Lagrange interpolation formula, and an inverse mapping is presented and proved. Application of the algorithm to matrix processors, specifically the rational matrix (a matrix whose elements are rational functions) inversion based on a division-free procedure and a procedure involving division is described. Some of the interesting results, *e.g.*, degree conditions for matrix processors, existence of a non-singular residue matrix with respect to a modulus, that are necessary to prove the applications of the algorithm to matrix processors are obtained.

A symmetrizer of a matrix A is a matrix X satisfying the matrix equation $XA = A^tX$ and $X = X^t$. A symmetrizer is useful in transforming a non-symmetric eigenvalue problem to a symmetric one. An algorithm for computing matrix symmetrizers valid only for Henenberg matrices with non-zero codiagonal was proposed by Datta[4]. An algorithm (general algorithm) which is valid for an arbitrary real non-symmetric matrix is obtained. It is shown that Datta's algorithm is a special case of the general algorithm. Also shown is that there exists no positive definite symmetrizer if the non-symmetric matrix has complex eigenvalues. In addition, a procedure which uses the general algorithm to compute equivalent symmetric matrices is proposed. An equivalent symmetric matrix of a real non-symmetric matrix is defined here as a real or a complex symmetric matrix whose eigenvalues are the same as those of the non-symmetric matrix. An implementation of the FLMAN on the general algorithm to compute a matrix symmetrizer exactly is also included.

A matrix T is symmetric Toeplitz if $t_{ij} = t_{|i-j|}$. If the leading minors of the non-singular Toeplitz matrix in a symmetric Toeplitz system of equations are zero or near zero then most of the algorithms for solving such a system fail or become unstable[5]. An algorithm that uses Zohar's formulation of Trench's algorithm which is an improvement of Levinson's algorithm to compute the inverse of a symmetric Toeplitz matrix, where the symmetric Toeplitz matrix can have vanishing or near-vanishing leading minors is proposed. In addition, the conventional single modulus residue arithmetic is superimposed on the foregoing algorithm to compute the exact inverse of a symmetric Toeplitz matrix with vanishing or near-vanishing leading minors.

A polynomial-time algorithm due to Barnes, which is a variation on Karmarkar's algorithm for linear programming, is studied. Proofs alternative to those of Barnes as well as some new results are obtained, specifically a result that ensures monotonic convergence of non-basic variables for a class of linear programming problems is proved. The detection of basic variables, based on the monotonic convergence of non-basic variables, as well as the problems involved therein, are discussed.

References

1. GREGORY, R. T. AND KRISHNAMURTHY, E. V. *Methods and applications of error-free computation*, 1984, Springer-Verlag.

2. BARNES, E. R. A variation on Karmarkar's algorithm for solving linear programming problems, *Math. Progm.*, 1986, **36**, 174–182.

3. GREGORY, R. T. *A finite number system for digital computers which gives exact results with rational operands, Tech. Rep.*, **CS-84-57**, Computer Science Department, University of Tennessee, Knoxville, TN 37916, July 1984.

4. DATTA, B. N. An algorithm for computing a symmetrizer of a Hessenberg matrix, unpublished.

5. BUNCH, J. R. Stability of methods for solving Toeplitz systems of equations, *SIAM J. Sci. Statist. Computing*, 1985, **6**, 349–364.

Thesis Abstract (Ph.D.)

Numerical studies of some flow problems in rotating laminar boundary layers by A. Chandra Sekar.
Research supervisor: G. Nath.
Department: Applied Mathematics.

1. Introduction

Studies pertaining to rotational flows, other than their inherent interest have many important applications in the field of meteorology, turbomachinery and astrophysics. The axially symmetric flow due to a rotating infinite disk in a fluid at rest[1] and the flow due to a fluid rotating rigidly far away over a stationary infinite disk[2] are the pioneering works in this field. In the former case, the disk acts like a centrifugal fan initiating a radial outflow thereby causing an axial inflow. In the latter case the sense of the secondary circulation is reversed with radial inflow accompanied by axial outflow. The unsteady rotating boundary layer flow over an infinite porous disk at rest with a magnetic field is studied for the cases of incompressible[3] and compressible fluids, the latter with disk rotation and no mass transfer. The unsteadiness is due to the fact that the angular velocity of the fluid changes with time (for the compressible case, the disk rotation is also time dependent). For the incompressible case, self-similar solutions are obtained when the angular velocity of the fluid is taken in a particular form. Zandbergen and Dijkstra[4] reviewed Von Karman swirling flows in an exhaustive manner.

The similarity solution for the rotational incompressible flow over a finite stationary disk was deduced[5] and was found valid in the region near the edge of the disk. The rotational flow over a finite disk at rest[6] was solved by line iteration and underrelaxation. The steady compressible rotational flow over a rotating finite disk is studied for the nonisothermal case.

Numerical solutions of laminar boundary layer flows about a rotating sphere in an axial stream were obtained recently[7]. The unsteady compressible boundary layer flow over a rotating sphere in forced flow is studied, the rotation of the sphere being time dependent.

The study of swirling flows is important for their wide-spread engineering applications such as swirl atomizers, cyclone separators, cyclone combusters and many other devices. The unsteady swirling boundary layer flow through a nozzle, diffuser and hydrocyclone is studied with variable viscosity. The unsteadiness in this case is imposed on the free-stream velocity.

2. Results and conclusions

The methods of solution employed are: (i) quasilinearization in combination with an implicit finite difference scheme, (ii) quasilinearization with Runge-Kutta-Gill method, and (iii) a finite difference version of Crank-Nicholson scheme with Newton's linearization.

For the accelerating case (semi-similar flow) the effect of time is to reduce the amplitudes of the oscillations of the velocity components. The velocity profiles except for the case of suction approach their free-stream values in an oscillatory manner Application of a magnetic field dampens these oscillations. Injection produces a deeper inflow layer and destabilizes the motion whereas suction and magnetic field have a stabilizing influence. The effect of a cold disk causes radial outflow to predominate over inflow while the tangential overshoot is either reduced or absent. For the case of a hot-and-slower rotating disk the thermal boundary layer is not very well defined as the axial velocity is directed away from the disk.

Non-oscillatory velocity profiles are found at the edge of the disk and its immediate neighbourhood while in the other regions radial oscillations and tangential overshoot are present. Tangential overshoot manifests first and is then followed by radial oscillations. The effect of reducing the rotation parameter is to increase the radial and tangential oscillations.

For the accelerating case in the rotating sphere problem, the effect of time is to advance the point of vanishing longitudinal shear stress further upstream. The effect of rotation exhibits similar behaviour. Skin-friction parameters at the wall increase with an increase in the wall temperature. Hotter the sphere greater is the meridional velocity and increased rotation also causes an increase in the meridional velocity.

For the nozzle overshooting in the longitudinal velocity is apparent only for the decelerating case while for the hydrocyclone and diffuser it appears in the steady solution itself.

References

1. VON KARMAN, T — *ZAMM*, 1921, **1**, 233–252.
2. BODEWADT, U. T. — *ZAMM*, 1940, **20**, 241–253.
3. CHANDRASEKAR, A. AND NATH, G. — *Int. J. Engng Sci.*, 1986, **24**, 1667–1680.
4. ZANDBERGEN, P. J. AND DIJKSTRA, D. — *Annu. Rev. Fluid Mech.*, 1987, **19**, 465–491.
5. STEWARTSON, K. — In *Boundary layer research*, 1958, pp. 59–71, Springer-Verlag.
6. VAN DE VOOREW, A. I., BOOT, E. F. F. AND STOUT, J. — *Q. J. Mech. Appl. Math.*, 1987, **40**, 15–32.
7. EL-SHAARAWI, M. A. I., EL-REFAIE, M. F. AND EL-BEDEAWI, S. A. — *Trans. ASME J Fluid Engng*, 1985, **107**, 97–104.

Thesis Abstract (Ph.D.)

Boundary element method applied to fluid flow problems by S. Sekar.
Research supervisor: G. Nath.
Department: Applied Mathematics.

This work studies fluid flow problems by the boundary (finite) element method (BEM). The widely used finite element method (FEM) has advantages of flexibility in choosing the shape and size of the elements, arbitrariness of the mesh structure and freedom of choice in approximating the formulae[1], but it requires very large core (memory) when applied to problems in fluid dynamics. BEM makes use of the existing analytical solutions while approximating the given equations, and the subsequent steps

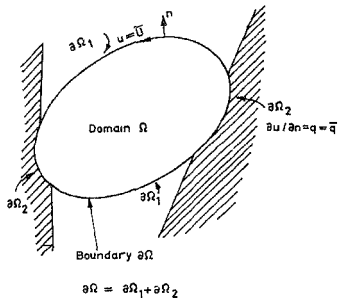

FIG. 1. Basic notation.

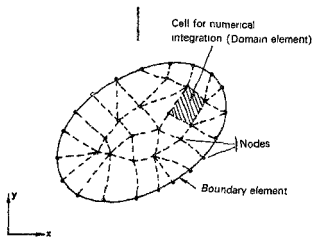

FIG. 2. Boundary element and internal cells or domain elements.

are similar to those of the FEM. Generally, BEM involves a transformation of the partial differential equation (describing the behaviour of the unknown variable in the domain Ω and on its boundary $\partial\Omega$) into an integral equation which relates only the boundary values (figs 1 and 2). Subsequently, the corresponding numerical approximation of the integral equation is evaluated, in a manner akin to that adopted in FEM, to obtain the values of the unknown variables at boundary nodes. The values of the unknown variables at internal points are calculated thereafter, wherever necessary, from the boundary data. A technique which has all the merits of the FEM, along with the additional benefit of reducing the dimensionality of the problem by one, is the BEM.

Chapter I presents a fairly extensive literature survey and introduces this method[2,3]. The advantages of BEM over other method numerical methods are brought out to justify its choice.

Chapter II deals with molecular diffusion in oscillating viscous flows in a pipe. The effect of flow oscillations on the axial diffusion of a solute in a pipe is analysed by the BEM. The governing equations are given by:

$$-\frac{1}{\rho}\frac{\partial p}{\partial x} = K\cos\omega t \quad \text{(the imposed pressure gradient)}$$

$$\frac{\partial U}{\partial t} = K\cos\omega t + \gamma\nabla^2 U \quad \text{(equation governing the viscous fluid flow)}$$

$$\frac{\partial c}{\partial t} + U\frac{\partial c}{\partial x} = D\nabla^2 C \quad \text{(convective molecular diffusion equation)}$$

with usual notation and appropriate boundary conditions, where K represents the magnitude of the oscillations, ρ the fluid density, D the diffusion coefficient, c the concentration. U is the velocity and ∇^2 the Laplacian operator, and x and t represent the space in axial direction and time variable.

The equation governing the fluid is solved analytically and using these results the nonlinear concentration equation coupled with fluid flow is solved by BEM, using the fundamental solution of the heat equation for a general initial distribution. The elements of the boundary and the domain are

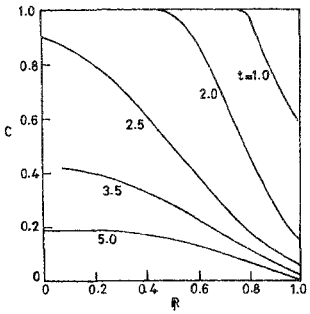

FIG. 3. Radial concentration profile for various times.

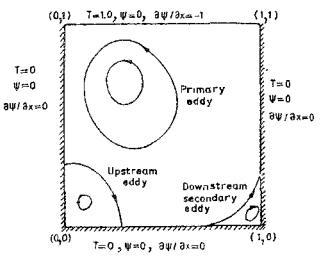

FIG. 4. A sketch of the coordinate system in a rectangular cavity.

generated as in the FEM and these integral equations are solved with linear variations, with the error analysis (fig. (3)).

In Chapter III, viscous flow in a square cavity, that is a flow induced by a steady motion of one of the walls in its own plane, and temperature distribution of the cavity are considered. The governing equations are

$$\nabla^2\psi = \omega$$

$$\nabla^2\omega = \mathrm{Re}\left[\frac{\partial\psi}{\partial y}\frac{\partial\omega}{\partial x} - \frac{\partial\psi}{\partial x}\frac{\partial\omega}{\partial y}\right]$$

$$\nabla^2\tau = \mathrm{Re}\,\mathrm{Pr}\left[\frac{\partial\psi}{\partial y}\frac{\partial T}{\partial x} - \frac{\partial\psi}{\partial x}\frac{\partial T}{\partial y}\right]$$

where Re is the Reynolds number, Pr the Prandtl number, and ψ, ω and T are stream function, vorticity and temperature, respectively. The boundary conditions are shown in fig. 4. The coupled equations are solved by modified biharmonic boundary element method by using two Green's functions G_1 and G_2. The eddy formation and the centre of the vorticity are analysed.

In Chapter IV, the steady and unsteady viscous flows in channels of variable cross-section are considered. With the usual notation the flow is governed by

$$\frac{\partial\omega}{\partial t} + \frac{\partial\psi}{\partial y}\frac{\partial\omega}{\partial x} - \frac{\partial\psi}{\partial x}\frac{\partial\omega}{\partial y} = \frac{1}{\mathrm{Re}}\nabla^2\omega + (\mathrm{Gr}/\mathrm{Re}^2)\frac{\partial T}{\partial x}$$

$$\frac{\partial T}{\partial t} + \frac{\partial\psi}{\partial y}\frac{\partial T}{\partial x} - \frac{\partial\psi}{\partial x}\frac{\partial T}{\partial y} = \frac{1}{\mathrm{Re.Pr}}\nabla^2 T$$

where Gr is the Grashoff number. New types of boundary conditions on vorticity are described and an unwind boundary element scheme is presented which increases the efficiency of the computational scheme. The scheme is given by a flow chart[1,2]. Using this method, extensive analysis is done to

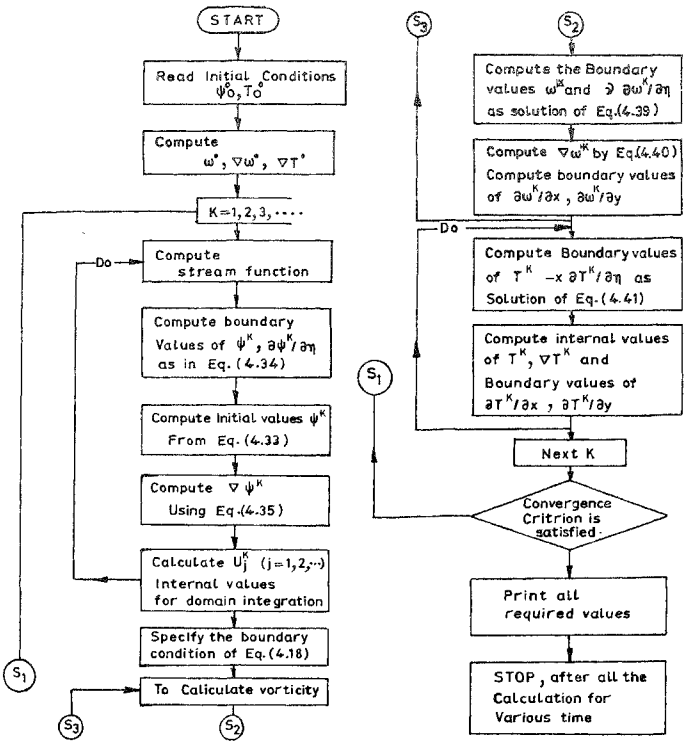

Flow chart.

calculate flow separation and reattachment in the stenosis region. For both steady and unsteady cases, flow separation analysis, pressure variation along the stenosis, and vorticity variation and reattachment were analysed to develop an insight into the growth mechanism of atherosclerosis, and consequently, to expedite its detection. Some of the results are presented in figs 5 and 6.

In the final chapter, to show the efficiency of the method, external flow, namely, two-dimensional flow around a cylinder, is considered. To make the method effective, a complex boundary element is considered to analyse the flow. After explaining the advantages and presenting error analysis for this method, some flow variables of interest are discussed in detail. The advantage of this method is that the approximation given by the complex variable boundary element method is an analytic function in

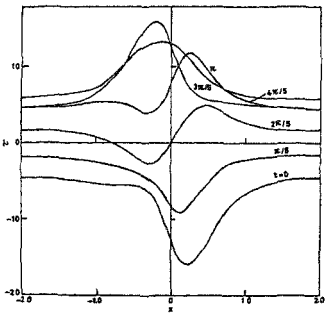

FIG. 5. Unsteady shear stress for various times $Re = 30$, model S_3.

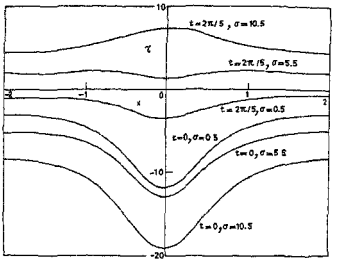

FIG. 6. Unsteady shear stress distribution for a locally constricted channel at various values of σ for $R = 0$.

the domain of interest and the integrals involved in the boundary element are solved exactly without using numerical approximations. This leads to minimisation in error.

References

1. CHUNG, T. J. — *Application of finite element method to fluid flow problems*, 1981, Pentagon Press.

2. BREBBIA, C. A. — *Topics in boundary element research*, Vols I and II, *Basic principles and applications*, 1984, Springer-Verlag.

3. BANERJEE, P. K. AND BUTTERFIELD, R. — *Boundary element method in engineering science*, 1981, McGraw-Hill.

Thesis Abstract (Ph.D.)

The swirling flows between rotating coaxial and non-coaxial disks by S. R. Kasiviswanathan.
Research supervisor: A. Ramachandra Rao.
Department: Applied Mathematics.

1. Introduction

Two special cases of interesting and intriguing rotating flow problems are the flow above an infinite rotating disk and between two infinite parallel disks rotating coaxially or non-coaxially. The credit for initiating research in this area goes to Theodore von Karman[1] who has considered the problem of the flow induced by an infinite rotating disk where the fluid far from the disk is at rest. By using a similarity principle, the full Navier-Stokes equations have been reduced to a pair of non-linear ordinary differential equations in the axial coordinate. Batchelor[2], Stewartson[3], and many other research workers have contributed a great deal to the problems of steady and unsteady flows. These studies involving rotating disks play a significant role in understanding the various phenomena

occurring in astrophysics, geophysical fluid dynamics, rheometry, lubrication and fabrication of computer memories by crystal, etc. Recently, the flow due to non-coaxially rotating disks has attracted the attention of many research workers after the pioneering work of Berker[4]. Breaking away from the approaches of von Karman and Batchelor which assumed axial symmetry, Berker has established the possibility of a new class of exact solutions in both coaxial and non-coaxial rotating disks in an ingenious way. These type of motions find application in understanding the flow in an instrument called orthogonal rheometer except that the disks being finite and many other situations of engineering interest. So far, there are no significant contributions dealing with the unsteady flows in the geometrical configuration of non-coaxial rotating disks.

2. Results and discussion

In this thesis an attempt is made to study some steady and unsteady flow problems due to single rotating disk and two disks rotating coaxially or non-coaxially in different fluid media in a variety of interesting situations. Interesting exact solutions are presented in most of the problems considered except in one in which a perturbation procedure is used.

In Chapter I, part A, the unsteady pseudoplane motions have been investigated in which each point of the parallel planes is subjected to non-torsional oscillations in its own plane and at any given instant the streamlines are concentric circles. Exact solutions are obtained and the form of the space curve Γ, the locus of the centres of these concentric circles, is discussed. The presence of three one-parameter family of exact solutions is established. For a symmetric solution of the flow these solutions reduce to a single unique solution. The nature of the curve Γ is illustrated graphically for some special cases. In Part B, an exact solution of the unsteady Navier-Stokes equations is obtained for the flow due to non-coaxial rotations of a porous disk, executing non-torsional oscillations in its own plane, and a fluid at infinity.

In Chapter II, Part A, exact solutions are obtained by using Laplace transform technique for the unsteady MHD flow of a viscous, electrically conducting, homogeneous, incompressible fluid between two infinite parallel, insulated porous disks rotating with the same angular velocity about two non-coincident axes. The disks are subjected to non-torsional oscillations of different frequencies and a uniform magnetic field is applied normal to the disks. Necessary and sufficient conditions for a solution to be symmetric and asymmetric are obtained. In Part B, the unsteady flow due to eccentric rotations of a single porous disk and a fluid at infinity which are subjected to non-torsional oscillations with different frequencies and a uniform magnetic field applied perpendicular to the disk is studied.

In Chapter III, Part A, the flow and heat transfer of an incompressible viscous fluid contained between two infinite parallel disks performing torsional oscillations of the same frequency, but rotating with different angular velocities about two non-coincident parallel axes where the disks are maintained at different temperatures are investigated. The governing equations are non-linear and the solution is obtained by a perturbation procedure with the parameter ε ($\ll 1$) the ratio of the angular velocity of the lower disk to the frequency of torsional oscillations of the disks. The corresponding heat transfer problem is studied and the solution is presented for temperature at zeroth order in ε. In Part B, the heat transfer problem corresponding to the flow problem presented in Part A of Chapter I is studied when the disks are maintained at steady or unsteady temperatures.

In Chapter IV, a class of exact solutions for the flow of a micropolar fluid between two infinite parallel non-coaxially rotating disks, is obtained. It is observed that a set of one-parameter family of exact solutions exists for the velocity and microrotation components. It is found that these infinite number of solutions for the velocity and microrotation components reduce to a single unique solution for a symmetric motion.

References

1. VON KARMAN, T. *ZAMM*, 1921, **1**, 233–252.
2. BATCHELOR, G. K. *Q. J. Mech. Appl. Math.*, 1951, **4**, 29–41.
3. STEWARTSON, K. *Proc. Camb. Phil. Soc.*, 1953; **49**, 333–341.
4. BERKER, R. *Int. J. Engng Sci.*, 1982, **20**, 217–230.

Thesis Abstract (Ph.D.)

Theoretical studies on some superconductors by R. Jagadish.
Research supervisor: K. P. Sinha.
Department: Applied Mathematics.

1. Introduction

Though the phenomenon of superconductivity was originally found in metals, it has since been found in a variety of alloys and compounds. It has also been found in compounds that exhibit long range magnetic order. The phenomenon of the coexistence of superconductivity and magnetism has been under study for the past two decades[1]. In this thesis we shall be partly concerned with the coexistence problem, in particular the coexistence of antiferromagnetism and superconductivity.

What has brought superconductivity into the limelight in the past few months is the discovery of high-temperature superconductors[2]. This new phenomenon is very poorly understood theoretically. Two possible mechanisms that can theoretically explain the high-temperature superconductivity phenomenon form the remaining work of the thesis.

2. Coexistence of antiferromagnetism and superconductivity

The coexistence problem has been tackled both microscopically and phenomenologically[3]. The microscopic mechanism involves the simultaneous creation or destruction of a Cooper pair and destruction or creation of two electrons at two neighbouring localized f-sites, with the f-electron system assumed to have perfect antiferromagnetic order. This interaction, in second order, is shown to produce an enhancement of the superconducting pairing. The upper critical field is calculated for the case of $SmRh_4B_4$ and is shown to agree satisfactorily with the experimental data. A Green's function calculation has been performed to explicitly show the interdependence of the superconducting and magnetic order parameters.

The phenomenological approach starts with a free-energy functional suitably modified to include the effects of magnetism. It is shown that the electrodynamic effects can only suppress the magnetic transition temperature and the upper critical field. The superconducting order parameter is also reduced due to the electrodynamic effects, when the magnetization is non-zero. On the other hand, the terms that directly couple the magnetization and the superconducting order parameter can act either way. In particular, when the coefficients of these direct coupling terms are negative, an enhancement of the magnetic transition temperature and the upper critical field results. The enhancement of the upper critical field in the case of $SmRh_4B_4$ has been demonstrated. It is shown that the superconducting order parameter is also enhanced, when the coefficients are negative, thus encouraging the coexistence. It has been suggested that the microscopic mechanism responsible for the negative values of the coefficients of the direct coupling terms is the one dealt with earlier.

3. High-temperature superconductivity

Of the two possible mechanisms suggested for the explanation of high-temperature superconductivity one involves the virtual exchange of electronic excitations[4]. The other involves the interaction of conduction electrons with the distortion field modes that are suggested to arise in the system due to structural instabilities which exist in the incipient state[5]. Although no detailed calculations have been attempted, it is shown that both the mechanisms can produce transition temperatures that are in the range of those of the new oxide superconductors.

References

1. SHRIVASTAVA, K. N. AND SINHA, K. P. *Phys. Rep.*, 1984, **115**, 93–149.
2. BEDNORZ, J. G. AND MULLER, K. A. *Z Phys. B*, 1986, **64**, 189–193.
3. JAGADISH, R. AND SINHA, K. P. *Pramāṇa*, 1987, **28**, 565–571.
4. JAGADISH, R. AND SINHA, K. P. *Curr. Sci.*, 1987, **56**, 291–292.
5. JAGADISH, R. AND SINHA, K. P. *Pramāṇa*, 1987, **28**, 317–319.

Thesis Abstract (Ph.D.)

Carbon and oxygen isotope studies of carbonates and graphites from Dharwar craton by B. Kumar.

Research supervisors: G. V. Anantha Iyer, A. G. Menon, Hari Narain (orgn).

Department: Physics.

1. Introduction

This thesis is concerned with studies of carbon and oxygen isotopes in carbonate and graphite samples from the Precambrian metasedimentary horizons of Dharwar craton, South India. The areas chosen for the present study include carbonate and graphite occurrences at Sargur, Bababudan, Chitradurga, Shimoga, Sandur and Kolar supracrustal belts. A total of 30 carbonate and 31 graphite analyses have been carried out in the present study, in addition to some major and minor elements (SiO_2, Al_2O_3, TiO_2, P_2O_5, MnO, Na_2O, K_2O, CaO, MgO, FeO, and Fe_2O_3) in the carbonates. The two-fold motivation of the present thesis is: (a) to interpret the carbon and oxygen isotopic data in the context of the sedimentary environment and to investigate the source of parent materials for the carbonates and graphites, and (b) to investigate the possible role of microorganisms in the sedimentation processes in the early Precambrian of the Dharwar craton.

2. C- and O-isotopes in carbonates

The C-isotope data of carbonates vary in a narrow range of -2.2 to $+0.3$ permil *vs* PDB with an overall mean of -0.7 ± 0.7 permil (n=29). $\delta^{13}C_{carb}$ mean for Sargur group is -1.2 ± 0.3 permil and for Chitradurga group -0.4 ± 0.6 permil. The oxygen isotope measurements for the carbonates give a $\delta^{18}O$ mean of $+16.2 \pm 3.2$ permil *vs* SMOW (n=29) with the values for the Sargur and Chitradurga groups being $+15.6 \pm 2.8$ permil and $+17.6 \pm 2.1$ permil, respectively. These data are within the range of isotopic ratios of Precambrian carbonates in other parts of the world[1,2]. In the

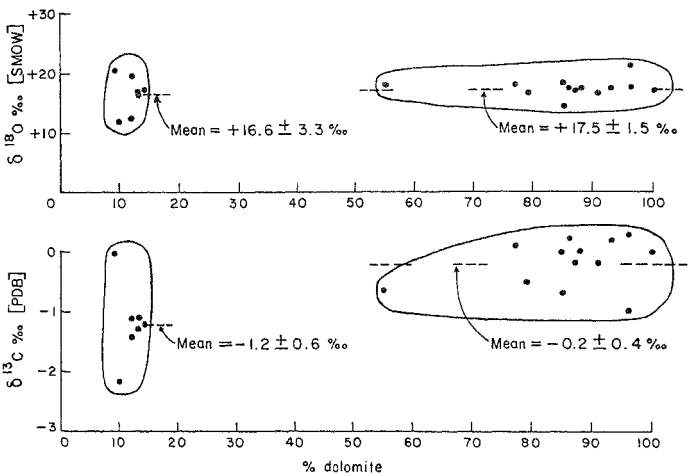

FIG. 1. $\delta^{13}C$ and $\delta^{18}O$ *vs* weight % of dolomite.

present study, two types of carbonates have been distinguished: (a) carbonates with dolomite of less than 14% (n=7) with a mean $\delta^{13}C$ value of -1.2 ± 0.6 permil *vs* PDB and a mean $\delta^{18}O$ value of $+16.6\pm3.3$ permil *vs* SMOW, and (b) carbonates with dolomite of greater than 50% (n=13) with a mean $\delta^{13}C$ value of -0.2 ± 0.4 permil and mean $\delta^{18}O$ value of $+17.5\pm1.5$ permil (fig. 1). Assuming that dolomitization of limestone was a process accompanying diagenesis and metamorphism, the data have been used to suggest that the source of carbonate-carbon was a large CO_2 reservoir which itself had a constant $\delta^{13}C$ value. This resulted in the narrower range of δ-values of the dolomitic limestones which were subsequently formed. The oxygen isotope ratios measured also support the above inference and they further suggest the existence of a large water body which restrained the scatter of dolomitic limestone δ-values within a narrow range.

3. C-isotopes in graphite

The $\delta^{13}C_{gr}$ values for graphites vary largely between -40.8 and -15.7 permil *vs* PDB with an overall mean of -27.9 ± 7 permil (n = 31). The Sargur group has $\delta^{13}C$ average of -23.6 ± 6.8 permil and the Dharwar supergroup average is -32.4 ± 4 permil. The large variation in the δ-values of graphite-carbon has been attributed to the fact that, unlike the carbonates, the process of graphitisation was controlled by local parameters and that the carbon reservoir for graphite was comparatively smaller. In addition, the $\delta^{13}C$ values also differed in the different reservoirs and isotopic exchange between the carbonate phase and the graphite phase in each reservoir did not take place.

4. Conclusion

With regard to the source of carbon in both the carbonates and graphites, there is a fair degree of certainty that the carbonate-carbon came from a predominantly inorganic source. It is not possible at this point to distinguish between the various sources—atmospheric CO_2, mantle-exhaled CO_2 and CO_2 from decarbonation of limestone—but it appears quite certain that all these sources influenced the $\delta^{13}C$ values of the carbonates. With reference to the graphite-carbon, it may be concluded that the $\delta^{13}C_{gr}$ values observed indicate the presence of a highly depleted source. This depleted source could either be an organic reservoir of reduced carbon or a reservoir largely controlled by solution chemical parameters which brought about such a large fractionation.

References

1. EICHMANN, R. AND SCHIDLOWSKI, M. — Isotopic fractionation between coexisting organic carbon-carbonate pairs in Precambrian sediments, *Geochim Cosmochim. Acta*, 1975, **39**, 585–595.

2. SCHIDLOWSKI, M., EICHMANN, R. AND JUNGE, C. E. — Precambrian sedimentary carbonates: carbon and oxygen isotope geochemistry and implications for the terrestrial oxygen budget, *Precambrian Res.*, 1975, **2**, 1–69

Thesis Abstract (Ph.D.)

Magnetic, electronic and superconducting properties of metal oxides of K_2NiF_4 and related structures by R. A. Mohan Ram.
Research supervisors: C. N. R. Rao and P. Ganguly.
Department: Solid State Structural Chemistry Unit.

1. Introduction

There has been considerable interest in recent years in the crystal chemistry and properties of layered metal oxides possessing K_2NiF_4 or related structures. The crystal chemistry of the oxides of the general formula A_2BO_4 with particular reference to the stability of the K_2NiF_4 structure have been discussed by Ganguly and Rao[1]. While K_2NiF_4 itself is a well-known two-dimensional antiferromagnet, oxides of this structure exhibit a variety of magnetic properties. Besides the ternary A_2BO_4 oxides, the structure and magnetic properties of some complex oxides where A or/and the B ions are partly substituted by other cations have been reported in the literature. Electrical properties of many of these oxides are significantly different from those of the corresponding three-dimensional perovskite oxides. For example, $La_{1-x}Sr_xVO_3$ is metallic when $0.3 < x < 0.05$, but $La_{1-x}Sr_{1+x}VO_4$ is insulating. Oxides of the K_2NiF_4 structure have become much more fascinating in the last few months because of the discovery of high-temperature superconductivity in some of the copper oxides of the type $La_{2-x}Sr_xCuO_4$ and $Y_{3-x}Ba_{3+x}Cu_6O_{14}$. In this thesis, electronic, magnetic and superconducting properties of several families of oxides possessing K_2NiF_4 and related structures are discussed.

2. Experimental

Various oxides with K_2NiF_4 and related structure have been prepared by ceramic method; stoichiometric amounts of the starting materials such as oxides, carbonates and/or oxalates were

weighed, grounded well and fired at high temperatures (1200–1700 K) or by coprecipitation method which involves the coprecipitation of the metal ions as carbonates or nitrates and decomposing them at temperatures as required (1000–1300 K). The oxides so formed were thoroughly ground, pelletised and sintered at suitable high temperatures.

All the oxides prepared were characterized by X-ray diffraction studies, magnetic susceptibility measurements, electrical resistivity measurements and infrared spectroscopic studies.

3. Results and discussion

Electrical and magnetic properties of $La_3Ni_2O_7$ and $La_4Ni_3O_{10}$ have been investigated in comparison with those of La_2NiO_4, $LaNiO_3$ and $LaSrNiO_4$. The results suggest an increasing three-dimensional character across the homologous series $La_{n+1}Ni_nO_{3n+1}$ with increase in n. Accordingly, the electrical resistivity decreases in the order $La_3Ni_2O_7$, $La_4Ni_3O_{10}$ and $LaNiO_3$ and this trend is likely to be related to the percolation threshold. Magnetic properties of these oxides also show interesting trends across the series[2].

In $LaSr_{1-x}Ba_xNiO_4$, the unit cell parameters (and unit cell volume) increase progressively with increase in x. The e_g electrons in these oxides seem to be in extended states forming a $\sigma^* x^2 - y^2$ band; with increase in x, the bandwidth decreases accompanying an increase in the unit cell volume. High-spin Ni^{3+} ions are formed to a small extent with increasing x, but there is no spin-state transition. Electrical and magnetic properties of these oxides are shown to be related.

$La_2CoO_{4+\delta}$ ($\delta \simeq 0.1$) possessing the K_2NiF_4 structure has been prepared by skull melting and ceramic method. The evidence for antiferromagnetic ordering has been found in these samples. Although we could prepare stoichiometric La_2CoO_4 by the reduction of the oxygen-excess samples, its complete characterization has not been possible.

Electrical and magnetic properties of several oxide systems of K_2NiF_4 structure have been compared with those of the corresponding perovskites. Quasi two-dimensional oxides of the $La_{1-x}Sr_{1+x}MnO_4$ system, possessing the K_2NiF_4 structure, show no evidence for ferromagnetic ordering in contrast to the corresponding three-dimensional $La_{1-x}Sr_xMnO_3$ pervoskites. Instead, there is an increasing tendency towards antiferromagnetic ordering with increasing x in $La_{1-x}Sr_{1+x}MnO_4$; furthermore, these oxides are relatively high-resistivity materials over the entire compositional range. Substitution of Ba for Sr in $La_{0.5}Sr_{1.5}MnO_4$ decreases the ferromagnetic interaction. Increasing the number of perovskite layers in $SrO.(La_{1-x}Sr_xMnO_3)_n$ causes an increase in electrical conductivity as well as ferromagnetic interaction. The oxide becomes a highly conducting ferromagnet when $n \geq 2$. Members of the $La_{1-x}Sr_{1+x}CoO_4$ system are all semiconductors with a high activation energy for conduction unlike $La_{1-x}Sr_xCoO_3$ ($x \geq 0.3$) which is metallic; the latter oxides are ferromagnetic. $La_{0.5}Sr_{1.5}CoO_4$ shows a magnetization of 0.5 μ_B at 0K (compared to 1.5 μ_B of $La_{0.5}Sr_{0.5}CoO_3$) but the high-temperature susceptibilities of the two systems are comparable. $LaSrMn_{0.5}Ni_{0.5}(Co_{0.5})O_4$ shows no evidence of long-range ferromagnetic ordering unlike the perovskite $LaMn_{0.5}Ni_{0.5}(Co_{0.5})O_3$; high-temperature susceptibility behaviour of these two insulating systems is however similar. Susceptibility measurements show no evidence for long-range ordering in $LaSrFe_{1-x}Ni_xO_4$ unlike the $LaFe_{1-x}Ni_xO_3$ ($x \leq 0.35$) and the electrical resistivity of the former is considerably higher. Electrical resistivity of Sr_2RuO_4 is more than an order of magnitude higher than that of $SrRuO_3$. Some generalization of the properties of two- and three-dimensional oxide systems have emerged from these experimental observations[3].

After the advent of superconductivity in La-Ba-Cu-O system[4], the phase responsible for superconductivity in this system has been found to possess the K_2NiF_4 structure. We have prepared and characterized several oxide systems such as $La_{2-x}Sr_x(Ba_x)CuO_4$, $La_{2-x}Sr_{x-y}Ba_y(Ca_y)CuO_4$ and

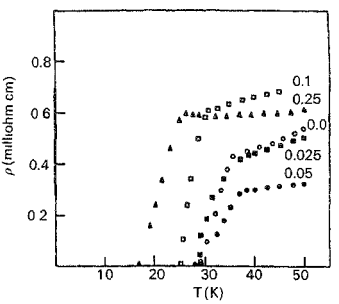

FIG. 1. Resistivity data of $(La_{1-y}Pr_y)_{1.8}\ Sr_{0.2}CuO_4$ (values of x are shown).

$(La_{1-y}Ln_y)_{2-x}Sr_x(Ba_x)CuO_4$ (Ln = Pr, Nd, Eu and Gd) possessing K_2NiF_4 structure which show superconductivity in the 15-40K region. In all these oxides it was found that the oxides $La_{1.8}Sr_{0.2}CuO_4$ and $La_{1.85}Ba_{0.15}CuO_4$ show highest T_c (onset around 40 and 30K and zero-resistance around 30 and 24K, respectively). Any substitution in these oxides such as Sr by Ca, Ba or La by Pr, Nd, Eu, Gd results in a decrease of superconducting transition temperature. A typical resistivity data of $(La_{1-y}Pr_y)_{1.8}Sr_{0.2}CuO_4$ is shown in fig. 1. All these oxides show marginal metallicity ($\rho \sim 10^{-2} - 10^{-3}$ ohm cm) at room temperature. The role of marginal metallicity of the non-superconducting phases and the nominal Cu^{3+}/Cu^{2+} ratio in making these oxides superconducting has been discussed[5]. We have observed that most of these oxides show superconductivity with high T_c (onset around 30K) around a critical a parameter of 3.780 ± 0.005Å and the c/a ratio of 3.50 ± 0.01. We have also prepared several other La-Ba-Cu-O and related oxides [*e.g.* $(La, M)_{n+1}Cu_nO_{3n+1}$ (M = Ba, Sr and y)] not possessing the K_2NiF_4 structure and studies show the absence of superconductivity in these oxides.

Soon after the discovery of the oxides of La-Ba(Sr)-Cu-O system we started investigating $La_3Ba_3Cu_6O_{14+\delta}$ oxide system and its Yttrium analogue. In the meantime there was a report that $Y_{1.2}Ba_{0.8}CuO_4$ is superconducting with zero-resistance around 83K and that this oxide is multiphasic. We investigated this system starting from the Y-Ba-Cu-O oxides analogous to $La_3Ba_3Cu_6O_{14}$ system, since Y_2CuO_4 does not form in the K_2NiF_4 structure. We observed superconductivity in various oxides of $Y_{3-x}Ba_{3+x}Cu_6O_{14}$ system above liquid – N_2 temperature; all these oxides were found to be biphasic consisting of a green and a black oxide[6]. The phase responsible for superconductivity in these oxides was identified to be $YBa_2Cu_3O_{7-\delta}$ (black oxide) and green phase was found to be insulating Y_2BaCuO_5. The $YBa_2Cu_3O_7$ (O_2-annealed) showed an onset of superconductivity around 120K and zero-resistance at 90 ± 2 K (fig. 2)[7]. This oxide showed 100% Meissner effect. We also observed that the thermopower of the superconducting $YBa_2Cu_3O_{7-\delta}$ suddenly goes to zero at 90K where zero-resistance is also attained. Based on the neutron-diffraction studies the structure of this perovskite-related oxide may be represented as shown in fig. 3. From one TGA studies we have shown that the oxygens in the middle CuO chains of $YBa_2Cu_3O_7$ are likely to be involved in the superconductivity[8]. These oxygens are found to be very crucial as heating this superconducting oxide in N_2 or in vacuum destroys the superconductivity because of the loss of the oxygen atoms from the

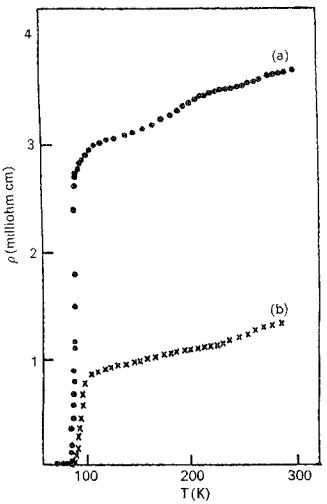

FIG. 2. (a) Resistivity data of $YBa_2Cu_3O_7$ (annealed in O_2 at 1100 K), (b) After prolonged annealing superconductivity is found at higher temperatures.

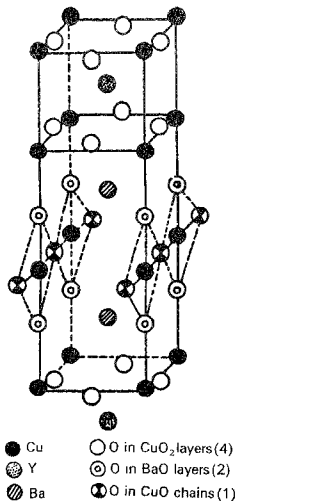

FIG. 3. Structure of $YBa_2Cu_3O_7$. The Y ions are separated by CuO_2, BaO, CuO, BaO and CuO_2 units. The middle CuO layer consists of strings of corner-shared $(CuO_4)_\infty$ units; three oxygens lie in a row between two such CuO_4 units.

middle CuO chains. We have attempted to substitute Y in $YBa_2Cu_3O_7$ by Er, Yb and other magnetic rare-earth ions and all these have been found to be superconducting above 77K[9]. The insensitivity of the superconducting behaviour towards the replacement of Y by other magnetic ions arises from the insulation of the middle layer (CuO chains) by BaO and CuO_2 layers on either side.

References

1. GANGULY, P. AND RAO, C. N. R. *J. Solid St. Chem.*, 1984, **53**, 193–216.
2. MOHAN RAM, R. A., GANAPATHI, L., GANGULY, P. AND RAO, C. N. R. *J. Solid St. Chem.*, 1986, **63**, 139–147.
3. RAO, C. N. R., GANGULY, P., SINGH, K. K. AND MOHAN RAM, R. A. *J. Solid St. Chem.*, 1988, **72**, 14–23.
4. BEDNORZ, J. G. AND MULLER, K. A. *Z. Phys. B*, 1986, **64**, 189–193.
5. MOHAN RAM, R. A., GANGULY, P. AND RAO, C. N. R. *Phase Transitions*, 1987, **10**, 107–

6.	MOHAN RAM, R. A., SREEDHAR, K., RAYCHAUDHURI, A. K., GANGULY, P. AND RAO, C. N. R.	*Phil. Mag. Lett.*, 1987, **55**, 257–263.
7.	RAO, C. N. R., GANGULY, P., RAYCHAUDHURI, A. K., MOHAN RAM, R. A. AND SREEDHAR, K.	*Nature*, 1987, **326**, 856–857.
8.	RAO, C. N. R., GANGULY, P., GOPALAKRISHNAN, J. AND SARMA, D. D.	*Mat. Res. Bull.*, 1987, **22**, 1159–1163.
9.	MOHAN RAM, R. A., VASANTHACHARYA, N. Y., GANGULY, P. AND RAO, C. N. R.	*J. Solid St. Chem.*, 1987, **69**, 186–188.

Thesis Abstract (Ph.D.)

Excited state behaviour of α, β-unsaturated thiones by V. Pushkara Rao.
Research supervisor: V. Ramamurthy.
Department: Organic Chemistry.

Thioenones, the formal analogues of enones, have received scant attention in comparison with the enones[1,2]. Considering the wealth of chemistry exhibited by enones[3,4], a systematic study on the thioenones should be of considerable interest. After a careful scrutiny of a large number of thioenones, a systematic investigation has been initiated on the excited state behaviour of thioenones **1–5**. Studies carried out on these systems are presented in this thesis.

In the photophysical study, the electronic absorption and emission characteristics and the behaviour of thione triplets using laser-flash photolysis were examined. The important features recognised in the photophysical behaviour of thioenones are: a) enhanced oscillatory strength for $S_0 \rightarrow T_1$ absorption, b) fluorescence from second-excited singlet state ($S_2 \rightarrow S_0$), c) phosphorescence from lowest triplet state ($T_1 \rightarrow S_0$), d) efficient quenching of triplet states by oxygen and ground-state thioenone (self-quenching), and e) high efficiency of intersystem crossing ($\Phi_{ISC} \sim 1$) and singlet oxygen generation ($\phi_{\Delta}^{T} \sim 1.0$).

Direct excitation of **1–5** in an aerated atmosphere into the $n\pi^*$ band results in the formation of the corresponding ketones. These thiones do not form the corresponding sulfines in the above oxidation although these are expected on the basis of the earlier studies on the oxidation of diaryl, arylalkyl and dialkyl thiones. The absence of sulfine in these cases is neither due to their instability nor due to their ready oxidizability as tested by independent experiments. The involvement of singlet oxygen as the oxidising species is suggested by the singlet-oxygen quenching and sensitisation experiments.

Formation of ketones appears to be preceded by a 1,2,3,-dioxathietane intermediate as the sulfur and sulfurdioxide products of its decomposition have been isolated in all the thiones investigated. This study demonstrates that thiocarbonyl chromophore is the site of attack by singlet oxygen in these cases and the adjacent C–C double bond is inert under these conditions.

The photochemical behaviour of thioenones towards both electron-rich and electron-poor olefins has been examined.

1

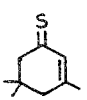

2

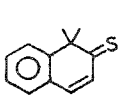

3

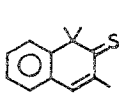

4

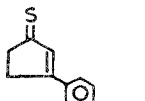

5

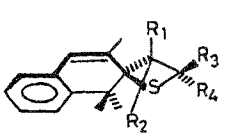

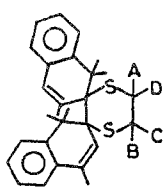

	R_1	R_2	R_3	R_4
6	CN	H	H	H
7	H	CN	H	H
8	CN	H	H	CH_3
9	CN	H	CH_3	H
10	CN	H	H	CN
11	CN	Cl	H	H
12	Cl	CN	H	H
13	CN	H	H	Ph
14	Ph	H	H	CN
15	$COCH_3$	H	H	H
16	H	$COCH_3$	H	H

	R_1	R_2	R_3	R_4
17	$COCH_3$	H	CH_3	CH_3
18	$COOCH_3$	H	H	H
19	$COOCH_3$	H	H	$COOCH_3$
20	OCH_2CH_3	H	H	H
21	OCH_2	H	CH_2	H
22	$OCOCH_3$	H	H	H
23	CH_3	CH_3	CH_3	CH_3
24	OCH_2	CH_2	H	H
25	OCH_2CH_3	H	H	H
26	$OCOCH_3$	H	H	H

Electron-deficient olefins add to thioenone **4** upon $\pi\pi^*$ excitation. Cycloaddition occurs to thiocarbonyl chromophore preferentially from the less-hindered side to yield thietanes (**6–19**). Thietane formation is stereospecific and regioselective. This addition is suggested to originate from the second-excited singlet state, $S_2(\pi\pi^*)$. Interestingly, the observed photochemical behaviour of thioenone towards electron-poor olefins is quite unique and is different from that of enones. Addition of electron-poor olefins to enones occurs at the olefinic centre to yield cyclobutanes and rarely does the oxetane formation compete.

Addition of electron-rich olefins to thioenone occurs at the thiocarbonyl chromophore to yield thietane (**20–23**) and 1,4-dithiane (**24–26**). The ratio of thietane *vs* dithiane is dependent on the conditions of irradiation and the nature of the olefin. This cycloaddition is suggested to originate from the lowest triplet state, $T_1(n\pi^*)$. 1,4-Prethietane biradical has been invoked as an intermediate (that being trapped by second molecule of thioenone to yield 1,4-dithiane). The results from the photocycloaddition of **4** to electron-rich olefins contrast sharply with those for photocycloaddition **4** to electron-poor olefins.

A systematic theoretical investigation was undertaken to understand the unique photochemical behaviour of thioenones towards olefins. This study forms a part of general attempt to predict both the thermal and photochemical behaviour of systems involving thiocarbonyl chromophore towards addends such as olefins and dienes. MINDO/3 calculations in conjunction with the well-known concepts of perturbation and frontier orbitals have been employed to make qualitative predictions of regioselectivity.

The PMO method in conjunction with MINDO/3 molecular orbital energies and coefficients are generally successful in rationalising the regiochemistry of thermal cycloadditions of thiocarbonyls The present analysis also leads to unequivocal predictions of regiochemistry for the thermal cycloadditions which have not been studied experimentally. The important predictions recognised are: thermal cycloaddition reactions of saturated thiones and 1-substituted dienes should be highly regioselective.

The prediction of reactivity ($n\pi^*$ *vs* $\pi\pi^*$-excited states) and regioselectivity of saturated thione in the photocycloadditions with electron-rich and electron-poor olefins are also in agreement with experimental results. Furthermore, the unique excited state behaviour of α,β-unsaturated thione towards electron-poor olefins is examined in this study. Evidence is presented for the important role of secondary orbital interactions in these systems. In conclusion, PMO model convincingly rationalised the three levels of selectivity observed in these systems: the preferred reaction site (C=C *vs* C=S), regiochemistry of the products (2,3-disubstituted thietane *vs* 2,2'-disubstituted thietane) and the preferred orientation of the substituents (cis *vs* trans).

References

1. RAMAMURTHY, V.	*Org. Photochem.*, 1985, **7**, 231–338.
2. DE MAYO, P.	*Acc. Chem. Res.*, 1976, **9**, 52–59.
3. EATON, P. E.	*Acc. Chem. Res.*, 1968, **1**, 50–57.
4. BALDWIN, S. W.	*Org. Photochem.*, 1981, **5**, 123–225.

Thesis Abstract (Ph.D.)

Structure-reactivity correlations in solid-state thermal and photochemical reactions by G. Satyanarayana Murthy.
Research supervisor: K. Venkatesan.
Department: Organic Chemistry.

1. Introduction

Single-crystal X-ray crystallographic investigations, analysis of the temperature factors for non-rigid body librations, Cambridge Structural Database analysis for crystal-engineering and lattice energy calculations to assess the importance of lattice relaxability in solid-state photochemical reactions are the highlights of the thesis.

2. Results and discussion

Chapter I discusses the crystal structures of derivatives of bishomocubane-dione molecule, (I) and (II) (fig. 1). Though the aim was to correlate the molecular geometry, especially the nature of four-membered rings in (I) and (II) with their different thermal reactivity[1], the presence of complex disorder exhibited by (II) did not allow to realise the original aim of the study. This molecule (II) in the lattice exhibits both enantiomeric and rotational disorders (fig. 2). Lattice energy calculations were in full agreement with the crystallographic interpretations of the nature of the disorder. Chapter II deals with variable temperature X-ray diffraction results of octachlorocyclophosphazene ($N_4P_4Cl_8$) in

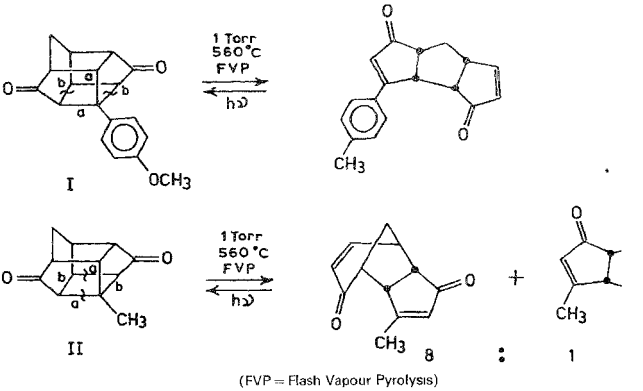

FIG. 1. Reactivities of molecules (I) and (II).

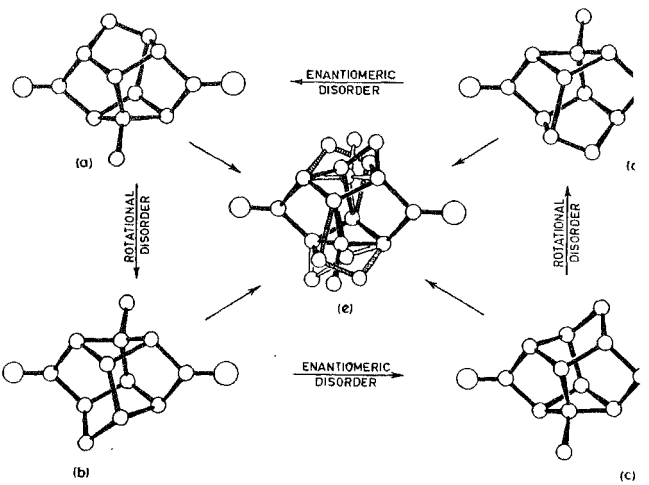

FIG. 2. Synthetic scheme involving the enantiomeric and rotational disorders in the crystals of compoun

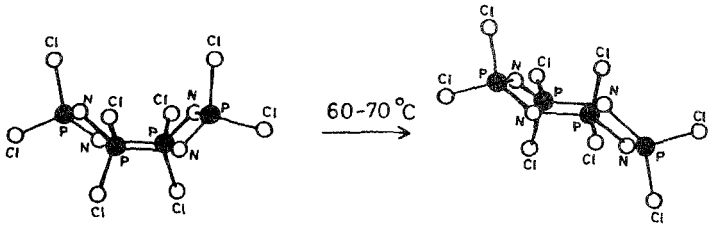

FIG. 3.

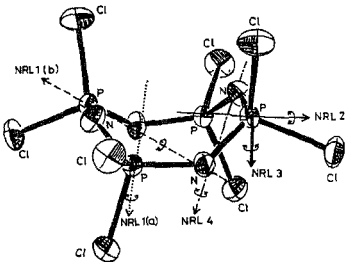

FIG. 4. Four types of non-rigid librations (NRL) analysed for $N_4P_4Cl_8$.

which the boat conformation with S_4 symmetry (K-form)[2] for the molecule changes to chair conformation with C_i-symmetry (T-form)[3] upon heating at about 60°C (fig. 3). Three different experiments, (i) observations under polarising microscope while heating the crystals, (ii) differential scanning calorimetry, and (iii) rotation photographs at different temperatures clearly indicate that the transformation takes place at ~ 55°C and it is single crystal → single crystal. Structures for K-form were determined at 25, 40 and 55°C and for T-form at 25°C. The temperature factors obtained from the least-square refinement for the K-form were analysed for their rigid- and non-rigid-body librational motions[4]. Of various models analysed, two of them (NRL2 and NRL4, fig. 4) were significant. These indicate that the motions of the nitrogen and PCl_2 groups perpendicular to the mean plane of the molecule lead to conformational isomerisation from boat to chair forms.

Chapter III discusses the crystal structure of tri-l-naphthylborane. This compound was reported[5] to exist in two polymorphs which interconvert upon heating. The compound, however, could be crystallised only from benzene and the crystals were unstable at atmospheric condition. The data were collected by mounting the crystals in Lindemann capillary tubes. Crystal structure solution indicated

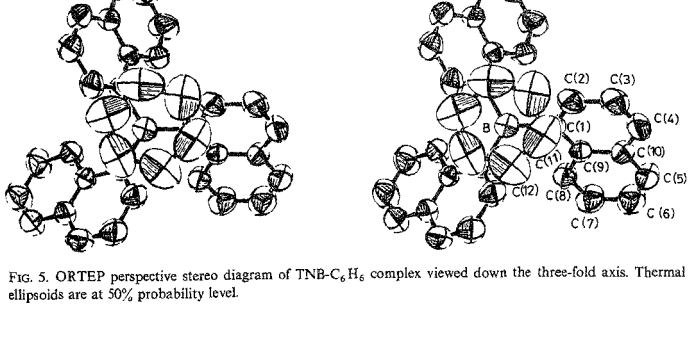

FIG. 5. ORTEP perspective stereo diagram of TNB-C_6H_6 complex viewed down the three-fold axis. Thermal ellipsoids are at 50% probability level.

that this compound forms a loose 1:1 complex with benzene and crystallises in a chiral space group R3 (fig. 5) undergoing 'spontaneous resolution'.

Chapter IV discusses the role of functional groups in 'crystal engineering'[6]. While coumarin itself is photostable in the solid state due to its unfavourable packing, chloro- and acetoxycoumarins are found to dimerise upon irradiation in the crystalline state. In this connection, X-ray crystallographic investigation of the photoreactive 6-acetoxycoumarin has been carried out. These molecules pack in the β-stacking mode with the shortest translational axis, $a = 3.90$ Å. The experimental data from the Cambridge Structural Database (CSD, 1981) for chloro- and acetoxy-substituted organic molecules have been analysed. This analysis showed that the chloro group has a preferential approach with either (i) $\theta_1 = \theta_2$ and $\chi = 180°$, (ii) $\theta_1 + \theta_2 = 180°$ and $\chi = 0°$ (fig 6); the former similar to α-type of packing which relates to the two interacting groups by a centre of symmetry and the latter corresponds to β-type of packing in which the interacting groups are related by transitional symmetry. As for acetoxy group containing systems, majority of the cases exhibit anti dipole–dipole interactions.

Chapter V deals with the question of the role of the lattice relaxibility in solid-state reactions. Topochemical postulates demand the two reactive double bonds in olefinic systems in the solid state to be parallely oriented and be within 4.2 Å to be photoreactive[7]. However, there are systems reported in recent years which apparently violated the topochemical rules[8]. The observation in 7-methoxycoumarin in which the double bonds are rotated about 67.5° is a typical example[9]. Though one expects these crystals to be photoinert, the dimerisation reaction is quite fast with yields as high as 90%. The rotational flexibility of molecules in the crystal lattice has been analysed by mapping the lattice energy with respect to the orientation angles θ_1, θ_2 and θ_3 and the displacements D_1 and D_2 (fig. 7). A number of systems were analysed which fall in the following categories: (i) properly juxtaposed and photoreactive, (ii) improperly juxtaposed and photoreactive, (iii) properly juxtaposed and photoinert, and (iv) improperly juxtaposed and photoinert. The increase in energy in (i) and (ii) after necessary molecular motions to achieve proper juxtaposition ($\theta_1 = 0°$, $\theta_2 = \theta_3 = 90°$) was significantly smaller compared to cases (iii) and (iv). This clearly demonstrates the important role of lattice relaxability for understanding the solid-state photochemical reactions.

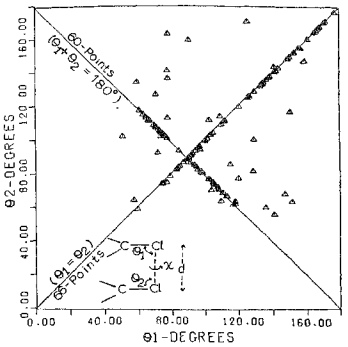

FIG. 6. Plot of θ_1 *vs* θ_2 for the unique Cl–Cl interactions. Points on the two diagonal lines represent α and β types of packing.

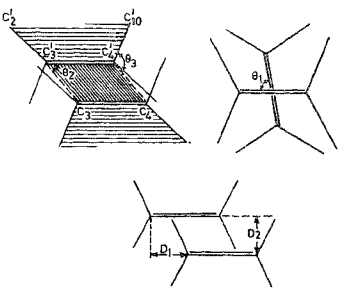

FIG. 7. Geometrical parameters used in the relative representation of reactive double bonds.

References

1. MEHTA, G., VEERA REDDY, A. AND SRIKRISHNA, A. — *J. Chem. Soc., Perkin Trans. I*, 1986, 291–297.
2. KETELAAR, J. A. A. AND DE VRIES, T. A. — *Rec. Trav. Chim. Pays-Bas*, 1939, **58**, 1081–1099.
3. HAZEKAMP, R., MIGCHELSEN, T. AND VOS, A. — *Acta Crystsllogr.*, 1962, **15**, 539–543.
4. WAGNER, A. J. AND VOS, A. — *Acta Crystallogr. B*, 1968, **24**, 707–713.
5. SCHOMAKER, J. AND TRUEBLOOD, K. N. — *Acta Crystallogr. A*, 1984, **40**, C339.
6. BROWN, H. C. AND SUJISHI, S. — *J. Am. Chem. Soc.*, 1948, **70**, 2793–2817.
7. SCHMIDT, G. M. J. — *Pure Appl. Chem.*, 1971, **24**, 647–678.
8. COHEN, M. D. AND SCHMIDT, G. M. J. — *J. Chem. Soc.*, 1964, 1996–2000.
9. MURTHY, G. S., ARJUNAN, P., VENKATESAN, K. AND RAMAMURTHY, V. — *Tetrahedron*, 1987, **43**, 1225–1240.
10. RAMASUBBU, N., GURU ROW, T. N., VENKATESAN, K., RAMAMURTHY, V. AND RAO, C. N. R. — *J. Chem. Soc. Chem. Commun.*, 1982, 178–179.

Thesis Abstract (M.Sc. (Engng))

Design, development and performance evaluation of differential temperature controller for solar thermal systems by G. K. Muralidhar.
Research supervisor: S. Mohan.
Department: Instrumentation and Services Unit.

1. Introduction

Solar energy, being one of the popular renewable energy sources, has its own diversified applications. Solar water heating is the most prominent and cost effective among the various applications of solar thermal energy. Solar water-heating (SWH) systems can be used either in thermosyphon (natural convection) mode or in forced circulation mode. Forced circulation systems, in which the fluid circulation is aided by a pump, require an automatic control for their efficient and economic operation.

Differential temperature controllers (DTCs) are incorporated into these systems to keep the pump operating only when sufficient energy is available for the collector. They control the operation of the pump by switching it ON and OFF depending on the temperature difference between the inlet and outlet, *i.e.*, the pump will be switched on whenever the temperature exceeds the high-set value called ΔT ON and switched off whenever it falls below the low-set value called ΔT OFF.

2. Design features

The present investigation concerns the design, development and performance evaluation of two models of differential temperature controllers.

The DTC (model 1) has been designed using a complete analog circuitry with locally available components with the following features[1]: (i) different modes of operation (ON-OFF-AUTO); (ii) remote temperature measurement and control; (iii) optional tank temperature high-limit protection; (iv) variable ΔT ON in the range 3.5 to 9.0°C; and (v) fixed ΔT OFF at 1.5°C.

This circuitry is later modified in order to have a thermostatic control for the back-up auxiliary heater used in systems where a constant outlet temperature is required, instead of tank temperature high-limit protection.

The second DTC (model 2) is developed using an imported integrated circuit with built-in control[2]. The main features of this controller are: (i) remote temperature measurement and control; (ii) tank temperature high-limit protection; (iii) optional thermostatic control; (iv) variable ΔT ON in the range 5 to 12°C; (v) variable ΔT OFF in the range 2 to 4.5°C; and (vi) temperature memory monitoring.

3. Experimental

These controllers are subjected to laboratory tests under simulated sensor conditions[3]. The set point variable potentiometers are calibrated in terms of temperatures. The set-point accuracies are tested on a 26 gal/day (100 LPD) capacity system. The first controller (model 1) showed better performance than the second controller (model 2). The stability of the set points at different inlet temperatures has been studied for both the controllers. Model 1 controller showed minimum variation in set points with temperature compared to the second one and the test results of the other

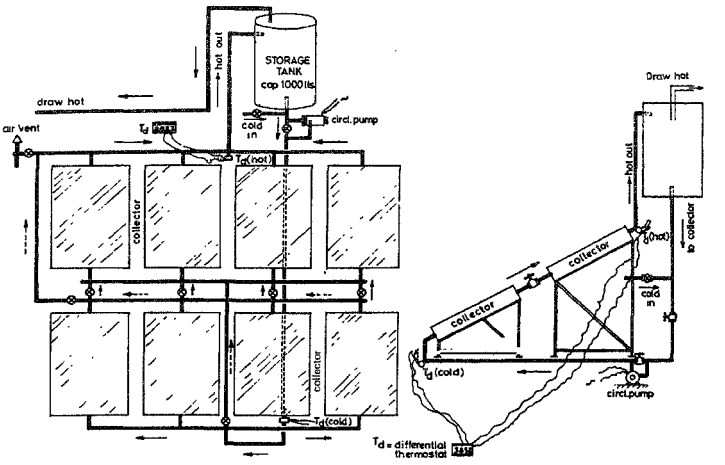

FIG. 1. 260 GPD Solar water-heating system.

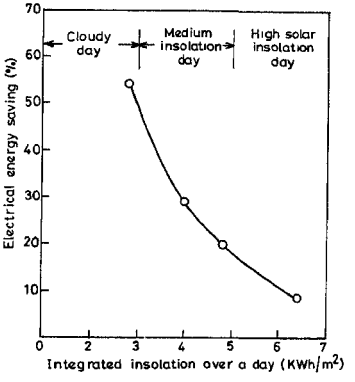

FIG. 2. Electrical energy savings using DTC.

controllers are reported in literature. However, model 2 with its additional features can be used for a number of other applications.

Finally the effectiveness of DTC on solar water-heating system performance has been studied on a 260 gal/day (1000 LPD) capacity system[4] as shown in fig. 1. The effect of flow rate on energy collection and pump cycling has been studied, keeping it at different values in the range 2 to 12 gal/min. The flow rate is optimised at 4 to 5 gal/min to get the maximum energy collection with reasonable rate of pump cycling. Then the influence of set points ΔT ON and ΔT OFF on pump cycling and energy collection has been investigated experimentally. The experimental results are compared with the analytical values obtained by Winn's method[5]. It has also been observed that ΔT OFF affects the system performance to a greater extent than ΔT ON. The electrical energy savings using the DTC have been found experimentally under different solar insolation and weather conditions. The electrical energy savings using the DTC are plotted as a function of insolation in fig. 2.

4. Conclusions

The present work is useful in that: (i) working models of two DTCs have been developed, (ii) the effectiveness of DTC on system performance has been studied experimentally.

References

1. MURALIDHAR, G. K., NAGARAJU, J. AND MOHAN, S. — A differential temperature controller for solar thermal system, *J. Instrum. Soc. India*, 1987, **17**, 267–273.
2. MURALIDHAR, G. K., NAGARAJU, J. AND MOHAN, S — A solar controller with a microprocessor based temperature monitor, *Proc. ISES Solar World Congress*, Hamburg, West Germany, 13–18, Sept., 1987.
3. MURALIDHAR, G. K., NAGARAJU, J. AND MOHAN, S. — Performance studies of a differential temperature controller for solar water heating system, *Proc. National Solar Energy Convention (NSEC-86)*, held at Madurai, 12–15, Sept., 1986.
4. MURALIDHAR, G. K., NAGARAJU, J. AND MOHAN, S. — The effectiveness of differential temperature controller – An experimental study, *ASME J. Solar Energy Engng* (communicated).
5. WINN, C. B. — The effects of temperature settings on cycling rates for bang–bang controllers, *ASME J. Solar Energy Engng*, 1984, **105**, 277–280.